Multiple Majorana edge modes in magnetic topological insulator–superconductor heterostructures

Qingming Li,[1,2] Yulei Han,[2] Kunhua Zhang,[2,3] Ying-Tao Zhang,[1,*] Jian-Jun Liu,[1,4,†] and Zhenhua Qiao[2,‡]

[1]*College of Physics, Hebei Normal University, Shijiazhuang, Hebei 050024, China*

[2]*ICQD, Hefei National Laboratory for Physical Sciences at Microscale, Chinese Academy of Sciences Key Laboratory of Strongly-Coupled Quantum Matter Physics, and Department of Physics, University of Science and Technology of China, Hefei, Anhui 230026, China*

[3]*School of Physics and Technology, Nanjing Normal University, Nanjing, 210023, China*

[4]*Department of Physics, Shijiazhuang University, Shijiazhuang, Hebei 050035, China*

(Received 16 August 2020; accepted 12 October 2020; published 3 November 2020)

We numerically investigate the electronic transport properties (i.e., electron tunneling and Andreev reflection) of a topological superconductor composed of a magnetic topological insulator and superconductors. A phase diagram is provided to distinguish various topological phases and their corresponding distinct Majorana edge modes. When superconductors are proximity coupled with the top and bottom surfaces of a magnetic topological insulator thin film, a quantum phase transition from topological insulator to quantum anomalous Hall effect passes through the regime possessing both chiral and helical edge modes. The hallmark feature is that the coefficient of electron tunneling is quantized to be $5/4$ and the remaining scattering processes exhibit an identical probability with a magnitude of $1/4$ in the coexisting states with a Chern number of $\mathcal{N} = \pm 1$. When the superconductors are proximity coupled with a nonmagnetic topological insulator thin film, we find that the perfectly quantized electron tunneling or crossed Andreev reflection can alternately appear via tuning the chemical potential.

DOI: 10.1103/PhysRevB.102.205402

I. INTRODUCTION

Majorana fermions, being their own antiparticles, can be realized as quasiparticles of topological states of quantum matter in condensed matter physics [1–5]. Because of the non-Abelian statistics and the nonlocality characteristic of Majorana fermions, the braiding of Majorana fermions is considered as the basic building block for fault-tolerant topological quantum computations [6–9]. So far, several proposed material systems were raised to realize such states, e.g., semiconductor-superconductor heterostructures [10,11], magnetic-atomic chains on top of superconductors [12,13], and topological insulators proximity coupled with superconductors [14–16]. Due to the superconducting proximity effect to the topological insulators, the corresponding heterostructures are also named after topological superconductors (TSCs). Depending on the time-reversal symmetry of the gapless boundary modes, topological superconductors can be classified into two different categories.

One is the "chiral" topological superconductor, in which the time-reversal symmetry is broken [17–20]. It possesses topologically protected chiral Majorana edge modes that can be analogous to the gapless edge modes of the quantum anomalous Hall effect [21–24], which is associated with a nonzero Chern number $\mathcal{C}$. From the view of topology, the quantum anomalous Hall effect with a Chern number of $\mathcal{C} = \pm 1$ is equivalent to the chiral topological superconductor with a Chern number of $\mathcal{N} = \pm 2$. And the $\mathcal{N} = \pm 1$ chiral topological superconductor can be realized when the system undergoes a topological phase transition from the quantum anomalous Hall effect to the normal Anderson insulator. The half-integer conductance plateau observed in a recent experiment had been used to be the evidence supporting Majorana fermions [25]. However, the subsequent theoretical and experimental interpretations imply that the half-integer conductance plateau is not sufficient evidence for the existence of a single chiral Majorana edge mode [26–28].

The other is the "helical" topological superconductor, in which the time-reversal symmetry is preserved [29–34]. It is characterized by a Z_2 topological index and possesses gapless helical Majorana edge modes, which are composed of two chiral Majorana edge modes with opposite chiralities, therefore also called the Majorana Kramers pair. By comparing the topological properties between the quantum anomalous Hall effect and chiral topological superconductor, it is natural to generalize the helical edge modes of the quantum spin-Hall insulator with twofold degrees of freedom to correspond to the helical topological superconducting edge states. Different from the chiral topological superconductor, the helical topological superconductor has yet to be observed in experiment.

Andreev reflection (AR) is an electron/hole transport process that occurs at the interface of a superconductor [35]. The local Andreev reflection converts an incident electron into a hole back to the same terminal, and a Cooper pair is created inside the superconductor [36–38]. The crossed Andreev reflection (CAR), also known as non-local Andreev reflection, is a nonlocal process describing the process of converting an electron incoming from one terminal into an outgoing hole to another spatially separated terminal [39–42]. Based on

*zhangyt@mail.hebtu.edu.cn

†liujj@mail.hebtu.edu.cn

‡qiao@ustc.edu.cn

crossed Andreev reflection, a Cooper pair in the superconductor can be split into two electrons propagating at two spatially separated terminals while keeping their spin and momentum entangled. These spatially separated entangled electrons are the key building blocks for solid-state Bell-inequality experiments, quantum teleportation, and quantum computation. The probability of crossed Andreev reflection is usually smaller than that of the local Andreev reflection. Therefore, how to increase the efficiency of Cooper-pair splitting (probability of crossed Andreev reflection) is crucial in engineering entangled electron states. With the discovery of topological materials, an intensive theoretical effort has been made in exploring the electron/hole transport properties in topological insulator–superconductor junctions, where high-efficiency Cooper-pair splitters were proposed to greatly enhance the crossed Andreev reflection and suppress other scattering processes [43,44]. However, these theoretical proposals mostly focused on the transport properties of the chiral topological superconducting mode, and are rarely devoted to the other topological superconducting modes.

In this paper, we investigate the topological superconductor with a Chern number of $\mathcal{N} = \pm 1$ to propose a topological state with coexisting chiral and helical Majorana edge modes. Compared to the quantum anomalous Hall effect, the quantum spin-Hall effect is topologically equivalent to a topological superconductor with two pairs of helical Majorana edge modes. Thus, by coupling the quantum anomalous Hall effect to the s-wave superconductors, the topological phase transition from the quantum anomalous Hall effect to the quantum spin-Hall effect may undergo a region with both chiral and helical Majorana edge states. In order to clearly understand the topological phase transition, we construct a system setup as displayed in Fig. 1 to study the electron tunneling (ET), AR, and CAR in the topological superconductor junction, where the left/right terminal is the quantum spin-Hall insulator, and the central scattering region is either the quantum anomalous Hall effect or quantum spin-Hall effect. We find that for the quantum anomalous Hall effect there exists a region with coexisting chiral and helical edge states, where the transport coefficients are, respectively, $T_{\rm ET} = 5/4$ and $T_{\rm AR} = T_{\rm CAR} = 1/4$; for the quantum spin-Hall effect, the quantized crossed Andreev reflection may appear by tuning the chemical potential via electric gating.

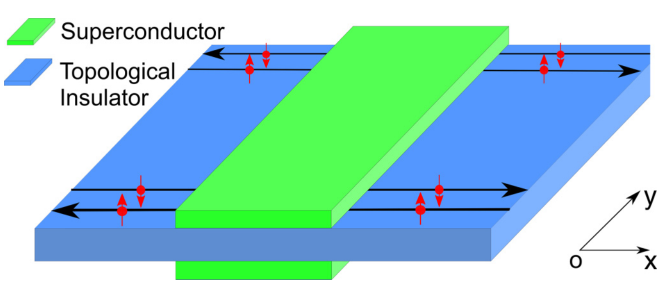

FIG. 1. Schematic plot of a two-terminal transport setup: In the central region, two superconductors are placed on top and bottom of a quantum spin-Hall insulator, while the left and right terminals are exactly extended from the quantum spin-Hall insulator. Note that in our paper the quantum spin-Hall insulator can be tuned to be the quantum anomalous Hall effect by introducing time-reversal breaking ferromagnetism. Black arrows denote the edge states, red circles indicate electrons, and upper/lower arrows represent the spin-up/-down states.

II. SYSTEM MODEL HAMILTONIAN

In our paper, we adopt the system of Bi_2Se_3 $\mathbb{Z}_2$ topological insulator thin films [45–47], and the corresponding quantum anomalous Hall insulator (or magnetic topological insulator) can be realized by introducing the ferromagnetic Cr and V atoms. Its low-energy effective Hamiltonian of the surface states near the Dirac point of the magnetic topological insulator thin film can be expressed as follows on the basis of $\psi_k = (c_{t\uparrow}, c_{t\downarrow}, c_{b\uparrow}, c_{b\downarrow})^T$:

$$H_0(k) = \upsilon_{\rm F}(k_y\sigma_x\tau_z - k_x\sigma_y\tau_z) + m(k)\tau_x + \lambda\sigma_z, \tag{1}$$

where t/b represents the top/bottom surface state; $\uparrow/\downarrow$ represents the spin-up/-down state; $\sigma_{x,y,z}$ and $\tau_{x,y,z}$ are, respectively, Pauli matrices in spin space and layers; and $\upsilon_{\rm F}$ is the Fermi velocity. The first term corresponds to the kinetic energy. The second term couples the top and the bottom surface states with $m(k) = m_0 + m_1(k_x^2 + k_y^2)$, where m_0 and m_1 are, respectively, the hybridization gap and the parabolic band component. The last term describes the exchange field along the z axis to break the time-reversal symmetry.

When the s-wave superconductors are proximately coupled with the topological insulator, a topological superconductor is produced and pairing potentials are induced. The corresponding Bogoliubov–de Gennes (BdG) Hamiltonian can be written as [18,33,48]

$$\mathcal{H}_{\rm BdG} = \sum_k \Psi_k^\dagger H_{\rm BdG}\Psi_k/2, \tag{2}$$

where $\Psi_k = [(c^t_{k\uparrow}, c^t_{k\downarrow}, c^b_{k\uparrow}, c^b_{k\uparrow}), (c^{t\dagger}_{-k\uparrow}, c^{t\dagger}_{-k\downarrow}, c^{b\dagger}_{-k\uparrow}, c^{b\dagger}_{-k\uparrow})]^T$ and

$$H_{\rm BdG} = \begin{pmatrix} H_0(k) - \mu_s & \Delta_k \\ \Delta_k^\dagger & -H_0^*(-k) + \mu_s \end{pmatrix}, \tag{3}$$

$$\Delta_k = \begin{pmatrix} i\Delta_1\sigma_y & 0 \\ 0 & i\Delta_2\sigma_y \end{pmatrix}, \tag{4}$$

where μ_s is the potential energy, and $\Delta_{1/2}$ are, respectively, the pairing gap functions on the top/bottom surface, respectively. To preserve the time-reversal symmetry, we set $\mu_s = 0$ and $\Delta_1 = -\Delta_2 = \Delta$, and the BdG Hamiltonian can be rewritten in a block-diagonal form:

$$H_{\rm BdG} = \begin{pmatrix} H_+(k) & 0 \\ 0 & H_-(k) \end{pmatrix}, \tag{5}$$

where $H_\pm(k) = \upsilon_F(k_y\sigma_x \mp k_x\sigma_y) + [m(k) \pm \lambda]\sigma_z\varsigma_z \mp \Delta\sigma_y\varsigma_y$ with $\varsigma_{x,y,z}$ being Pauli matrices in the Nambu space. The BdG Hamiltonian can therefore be decoupled into two parts with opposite chiralities, and the new basis in Eq. (5) becomes $(c^t_{k\uparrow} + c^b_{k\uparrow}, c^t_{k\downarrow} - c^b_{k\downarrow}, c^{t\dagger}_{-k\uparrow} + c^{b\dagger}_{-k\uparrow}, c^{t\dagger}_{-k\downarrow} - c^{b\dagger}_{-k\downarrow})^T/\sqrt{2}$ for $H_+(k)$ and $(c^t_{k\downarrow} + c^b_{k\downarrow}, c^t_{k\uparrow} - c^b_{k\uparrow}, c^{t\dagger}_{-k\downarrow} + c^{b\dagger}_{-k\downarrow}, c^{t\dagger}_{-k\uparrow} - c^{b\dagger}_{-k\uparrow})^T/\sqrt{2}$ for $H_-(k)$.

Note that the number of edge modes of the topological superconductor is determined by the Chern numbers $\mathcal{N}_+$ and $\mathcal{N}_-$ of the block-diagonalized Hamiltonians rather than the

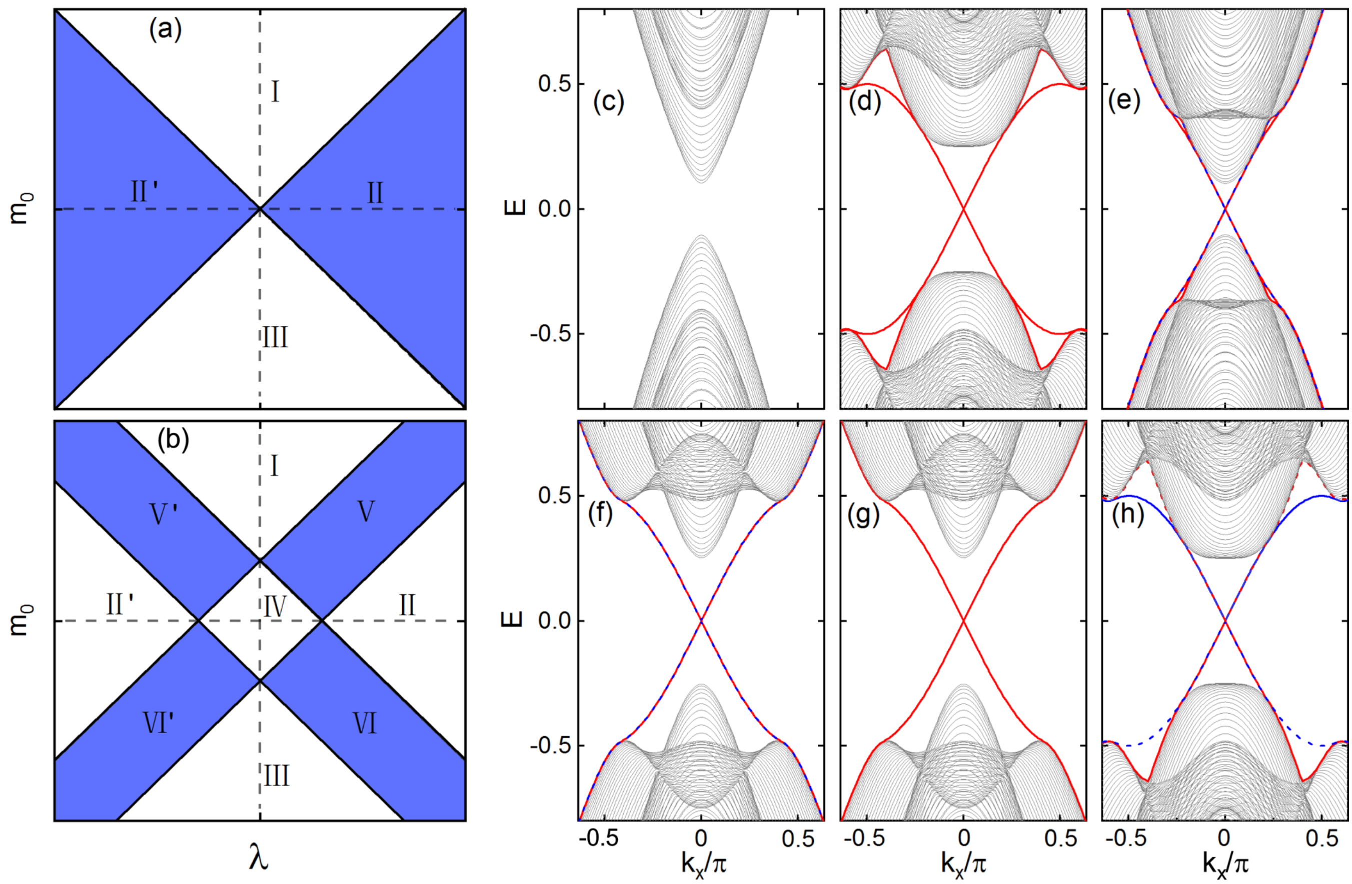

FIG. 2. (a) Phase diagram of the magnetic topological insulator thin films in the plane of exchange field λ and mass m_0. (b) Phase diagram of the proximity coupled magnetic topological insulator thin films in the plane of exchange field λ and mass m_0 at fixed $\Delta_1 = -\Delta_2 = \Delta$ and $\mu_s = 0$. The phase boundaries intersect at four points: $(0, \Delta)$, $(0, -\Delta)$, $(\Delta, 0)$, and $(-\Delta, 0)$ in the (λ, m_0) plane. (c–h) Corresponding band structures (or *energy spectra*) of the I-VI regions as displayed in panel (b). The parameters are set to be $m_0 = 0.5$ in panels (c), (d), and (g) and $m_0 = -0.5$ in panels (e), (f), and (h); $\Delta = 1$ in panels (d) and (f)–(h); $\Delta = 0.3$ in panels (c) and (e); $\lambda = 0$ in panels (c), (e), and (f); $\lambda = 1$ in panels (g) and (h); and $\lambda = 2$ in panel (d). The red and blue lines represent the direction of propagation of Majorana fermions at the system boundary, respectively.

total Chern number of $\mathcal{N} = \mathcal{N}_+ + \mathcal{N}_-$, where $\mathcal{N}_{+/-}$ is the Chern number of $H_{+/-}(k)$. For example, the topological state with a total Chern number of $\mathcal{N} = 1$ can be composed of $\mathcal{N}_{+/-} = 0/1$ or $-1/+2$. For the former case, the topological superconductor possesses a single chiral Majorana edge mode, while for the latter case the Chern number $\mathcal{N}_- = 2$ from $H_-(k)$ corresponds to a pair of edge modes with same chirality, while the Chern number $\mathcal{N}_+ = -1$ from $H_+(k)$ corresponds to a single edge mode with the opposite chirality. For concise and accurate description, the edge modes with Chern numbers $\mathcal{N}_{+/-} = -1/+2$ are named after the coexistence of chiral and helical Majorana edge modes.

When an electron comes from the left terminal, the electronic transport properties, i.e., the direct electron-tunneling coefficient T_{ET}, the Andreev reflection coefficient T_{AR}, and the crossed Andreev reflection coefficient T_{CAR}, can be numerically evaluated by [49]

$$T_{\mathrm{ET}} = \mathrm{Tr}\big[\Gamma^R_{ee} G^r_{ee} \Gamma^L_{ee} G^a_{ee}\big],$$
$$T_{\mathrm{AR}} = \mathrm{Tr}\big[\Gamma^L_{ee} G^r_{eh} \Gamma^L_{hh} G^a_{he}\big],$$
$$T_{\mathrm{CAR}} = \mathrm{Tr}\big[\Gamma^R_{ee} G^r_{eh} \Gamma^L_{hh} G^a_{he}\big],$$

where e/h represent the electron and hole, respectively. $\Gamma^{L/R}(E) = i[\Sigma^r_{L/R} - \Sigma^a_{L/R}]$ are the linewidth functions coupling the left/right terminals with the central scattering region. $G^r(E) = [E - H - \Sigma^r_L - \Sigma^r_R]^{-1}$ is the retarded Green's function and H is the BdG Hamiltonian in the tight-binding representation.

III. ENERGY SPECTRA AND PHASE DIAGRAMS

Let us first study the phase diagram of the magnetic topological system described in Eq. (1). Since the topological phase transition usually occurs when the bulk band gap closes and reopens, one can determine the phase boundaries by solving the band-crossing condition $E(k) = \pm\sqrt{\upsilon_{\mathrm{F}}^2 k^2 \pm [m(k) \pm \lambda]^2} = 0$. As displayed in Fig. 2(a), the phase diagram in the (λ, m_0) plane can be divided into four topologically different regimes by two-phase boundaries $m_0 = \pm\lambda$. For the case of $|m_0| < |\lambda|$, regions II and II' are, respectively, the quantum anomalous Hall phases with Chern numbers of $\mathcal{C} = \pm 1$. For the case of $|m_0| > |\lambda|$, the Chern number is $\mathcal{C} = 0$, with region I being a trivial insulator and region III being a quantum spin-Hall insulator [50].

Next, we consider the hybrid system with the s-wave superconductor proximity coupled with a magnetic topological insulator. At fixed $\mu_s = 0$, $m_1 = 1$, and $\Delta_1 = -\Delta_2 = \Delta$, the energy dispersion is $E(k) = \pm\sqrt{\upsilon_F^2 k^2 + \{\lambda \pm [m(k) \pm \Delta]\}^2}$, and the band gap closes at the Γ point for $\Delta \pm (m_0 \pm \lambda) = 0$. Figure 2(b) displays the phase diagram of the topological superconducting system. The four-phase boundaries separate the (λ, m_0) plane into nine gapped regions, including six different topological phases. The intersections of all phase boundaries, falling into the coordinate axis, yield the multicritical points that are closely related to Δ. To confirm the phase diagram from the bulk-edge correspondence, we investigate the band spectra of the superconducting nanoribbon with periodic boundary condition along the x direction and open boundary condition along the y direction. The topological phases with the corresponding band spectra are, respectively, characterized by the following.

(i) For $m_0 > |\lambda| + \Delta$ as shown in region I, it is the normal superconducting phase with a Chern number of $\mathcal{N} = 0$. This superconducting phase is adiabatically connected with the trivial insulator that is shown in region I of Fig. 2(a). In the corresponding band structure displayed in Fig. 2(c), a finite band gap opens without gapless edge states.

(ii) For $|m_0| < |\lambda| - \Delta$, when the superconducting proximity effect is infinitesimal, the weak pairing strength drives the quantum anomalous Hall phase with the Chern number of $\mathcal{C} = \pm 1$ [corresponding to the II (II') region in Fig. 2(a)] into the superconducting phase with a Chern number of $\mathcal{N} = \pm 2$, as displayed in the II (II') region of Fig. 2(b). From the corresponding band structure shown in Fig. 2(d), one can see that two pairs of Majorana edge modes with the same chirality emerge at both sides of the topological superconducting ribbon.

(iii) For $m_0 < -|\lambda| - \Delta$ as displayed in region III, it is a $\mathcal{N} = 0$ superconducting phase, that is adiabatically connected with the quantum spin-Hall phase [corresponding to region III in Fig. 2(a)]. As discussed above, a quantum anomalous Hall state is topologically equivalent to two pairs of Majorana edge modes with the same chirality. Therefore, in the presence of superconducting proximity effect, the quantum spin-Hall state can be naturally considered as a superconductor with two pairs of helical Majorana edge states. Due to even pairs of helical Majorana edge modes, according to the classification of Z_2 topological invariants, the class of DIII superconductor with Z_2 index $\nu = 0$ is topologically trivial. The band structures of the two pairs of helical states can be observed in Fig. 2(e).

(iv) For $|m_0| < \Delta - |\lambda|$ as displayed in region IV, due to the s-wave superconducting proximity coupling, the transition from the normal insulator to the quantum spin-Hall insulator should pass through a helical topological superconductor with the Chern number $\mathcal{N} = 0$. In the special case of $\lambda = 0$, two Majorana edge modes with opposite chiralities localizing at one edge of the topological superconductor form a Kramers pair, which is protected by the time-reversal symmetry. In the case of $\lambda \neq 0$ in region IV, although weak magnetic doping breaks the time-reversal symmetry, the system is still adiabatically connected with the helical topological superconductor that is protected by time-reversal symmetry. It is known that the phase transition from the time-reversal-invariant phase to a trivial superconducting phase cannot occur without the band gap closing and reopening [51]. According to the classification of Z_2 topological invariants, the class of DIII superconductor with Z_2 index $\nu = 1$ is topologically nontrivial. The band structure of the helical topological superconductor is displayed in Fig. 2(f). One can see that the top and bottom bands are separated by a gap and two pairs of counterpropagating edge modes with opposite chirality emerge at both sides of the ribbon.

(v) For $||\lambda| - \Delta| < m_0 < |\lambda| + \Delta$ shown in region V (V'), a $\mathcal{N} = \pm 1$ chiral topological superconducting phase emerges during the topological phase transition from a quantum anomalous Hall insulator to a trivial insulator. The corresponding band structure is shown in Fig. 2(g). One can find that a pair of chiral gapless edge state modes traverses across the Γ point, which holds a chiral Majorana mode.

(vi) For $-|\lambda| - \Delta < m_0 < -||\lambda| - \Delta|$ shown in region VI (VI'), there exist chiral and helical Majorana edge states with Chern number $\mathcal{N} = \pm 1$. Physically, the quantum spin-Hall insulator is topologically equivalent to the superconductor with two pairs of helical Majorana edge states, and the chiral topological superconductor with Chern number $\mathcal{N} = 2$ is topologically equivalent to the quantum anomalous Hall insulator. When considering the topological phase transition between quantum spin-Hall insulator and quantum anomalous Hall insulator, the superconducting proximity effect annihilates one chiral edge state and gives rise to the coexistence of chiral and helical Majorana edge states. The band structure of such coexisting states is displayed in Fig. 2(h). One can see that three pairs of gapless edge states traverse across the Γ point, propagating along both sides of the topological superconductor.

IV. ELECTRONIC TRANSPORT AND NUMERICAL ANALYSIS

To identify the various types of Majorana edge modes in our topological superconducting system, we investigate the quantum tunneling and Andreev reflection in the topological superconductor composed of quantum spin-Hall insulator and superconductor. The central region of our system setup is a quantum spin-Hall insulator proximity coupled with two s-wave superconductors with opposite signs of the pairing functions at the top and bottom surfaces, and the left/right terminals are the exact extension of the quantum spin-Hall insulator region, as displayed in Fig. 1. In order to clearly illustrate the electron/hole transport processes, the edge state configurations of the topological superconductor are plotted in Fig. 3. Due to the topological equivalence, the helical edge modes of the quantum spin-Hall insulator are split into four Majorana edge modes at the left and right terminals. Half of the Majorana edge modes with the same chirality from the upper block of Eq. (5) propagate along one direction, while the remaining Majorana edge states from the lower block of Eq. (5) propagate along the opposite direction. As discussed in the previous section, the variation of the exchange field λ or the hybridization gap m_0 can result in a series of topological phase transitions, which can be uniquely reflected from the edge state transport features.

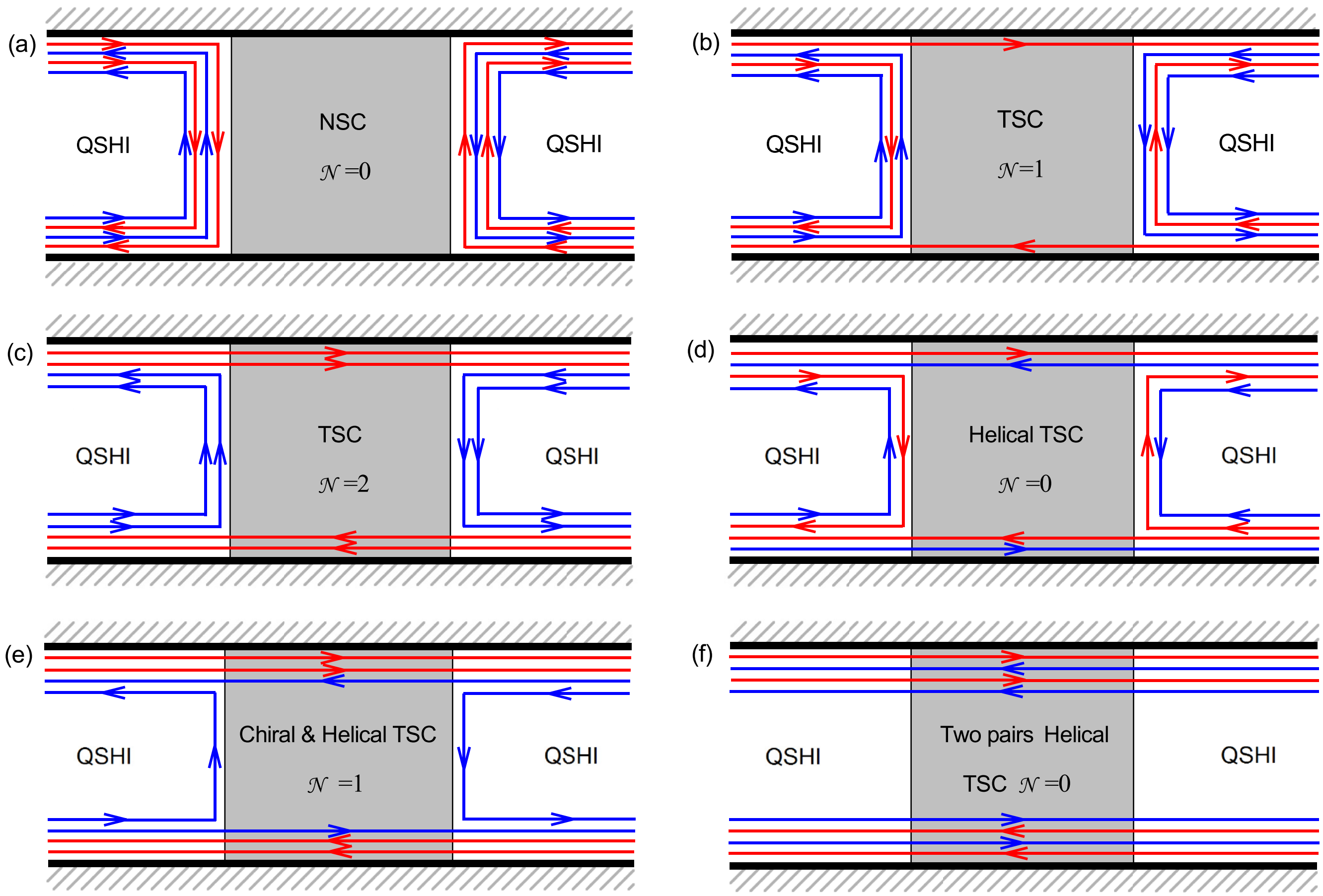

FIG. 3. Schematic plot of edge mode transport in the setup shown in Fig. 1. The central TSC region is set to be (a) the $\mathcal{N} = 0$ normal superconductor, (b) the $\mathcal{N} = 1$ topological superconducting edge mode, (c) $\mathcal{N} = 2$ topological superconducting edge modes, (d) $\mathcal{N} = 0$ helical topological superconducting edge modes, (e) coexisting chiral and helical edge modes, and (f) $\mathcal{N} = 0$ two-pair helical edge modes. Blue and red arrows indicate, respectively, Majorana edge modes with opposite chirality.

In Fig. 4(a), at fixed $\Delta = 0.3$ and $m_0 = 0.5$, the Chern number of the topological superconductor is $\mathcal{N} = \pm 2$ for $|\lambda| > 0.8$, $\mathcal{N} = \pm 1$ for $0.2 < |\lambda| < 0.8$, and $\mathcal{N} = 0$ for $|\lambda| < 0.2$. When $\mathcal{N} = \pm 2$ is chosen in the central region of our considered system, two chiral Majorana edge modes propagate along the system boundaries; i.e., in Fig. 3(c) one pair of Majorana edge modes propagates along the boundaries of the central region with the same chirality, while other edge modes are scattered back at the interfaces between the central region and terminals. Due to the fact that two Majorana edge modes with the same chirality can be combined into one quantum anomalous Hall state, such configuration is topologically equivalent to the quantum spin-Hall insulator–quantum anomalous Hall insulator junction. Therefore, the electron-tunneling coefficient is $T_{\rm ET} = 1$, and other transport coefficients are zero.

When the exchange field decreases, a topological phase transition occurs, leading to $\mathcal{N} = \pm 1$ with one Majorana edge state being destroyed. As displayed in Fig. 3(b), one can see that two edge modes, the propagating direction of which is opposite to the chiral edge mode in the central region, cannot transit through the central scattering region, while the other two edge modes, the propagating direction of which is the same as that of the chiral edge modes in the central region, are split into two chiral Majorana modes with one branch of chiral Majorana edge modes being perfectly transmitted but the other branch being perfectly reflected. Since the single chiral Majorana edge mode can be considered as half of the identical copies of the quantum anomalous Hall edge mode and contributes equally to the electron transport and Andreev scattering, one can get $T_{\rm ET} = T_{\rm LAR} = T_{\rm CAR} = 1/4$ [17,18].

When the exchange field further decreases, the central region is driven into the $\mathcal{N} = 0$ normal superconducting phase. Figure 3(a) displays that all the edge modes are completely reflected at the interface between the central region and the left terminal. As a result, all the electron tunneling $T_{\rm ET}$, Andreev reflection $T_{\rm AR}$, and crossed Andreev reflection are vanishing.

In addition to the exchange field, the hybridization gap (m_0) is also crucial to control the topological phase transitions. In the case of $m_0 = -0.5$, although the Chern number of topological superconductors in the central scattering region has not been changed, the corresponding number of edge states and the transmission coefficients are significantly different from the case of $m_0 = 0.5$. Figure 4(b) plots the transmission coefficients as functions of the exchange field λ at fixed $\Delta = 0.3$ and $m_0 = -0.5$. When $|\lambda| < 0.2$, two pairs of helical Majorana edge states are present in the topological superconducting region, as displayed in Fig. 3(f). Since

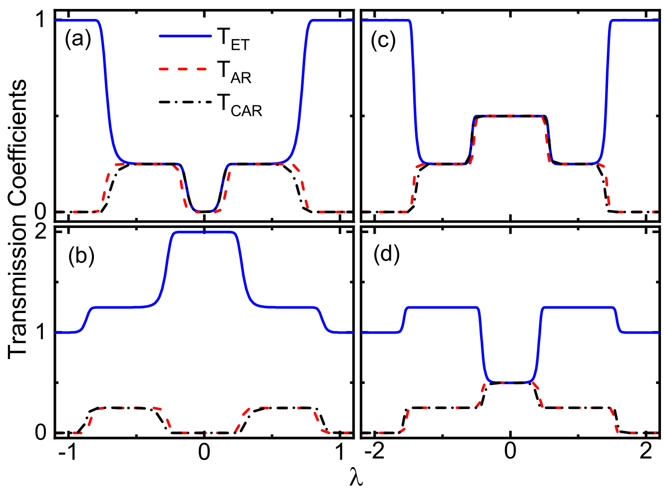

FIG. 4. Transmission coefficients of electron tunneling $T_{\rm ET}$, Andreev reflection $T_{\rm AR}$, and crossed Andreev reflection $T_{\rm CAR}$ vs exchange field λ in the topological superconductor with the energy $E = 0$ of the incident electron. $\Delta_1 = -\Delta_2 = 0.3$ for panels (a) and (b); $\Delta_1 = -\Delta_2 = 1$ for panels (c) and (d). $m_0 = 0.5$ for panels (a) and (c); $m_0 = -0.5$ for panels (b) and (d). The length of the central TSC is $L = 30$, and the ribbon width is $N = 120$.

these edge modes are topologically equivalent to the quantum spin-Hall edge modes, all the incoming edge modes from the terminals are perfectly transmitted, giving rise to $T_{\rm ET} = 2$ and $T_{\rm AR} = T_{\rm CAR} = 0$. To be specific, as the exchange field is within the range of $0.2 < |\lambda| < 0.8$, the superconducting region experiences a topological phase transition with one Majorana edge state emerging into the bulk, consequently leaving three Majorana edge states with odd Chern number $\mathcal{N} = \pm 1$. When such edge states exist in the central topological superconducting region, one can see that two Majorana edge modes with the same propagation direction combined with another Majorana edge mode propagating along the opposite direction form coexisting edge states appearing at the interface between the topological superconductor and vacuum, as displayed in Fig. 3(e). The two edge channels with the same chirality pass through the central scattering region and contribute to the tunneling coefficient with a value of 1, while another Majorana edge current in the opposite direction also passes through the central scattering region, leading to $T_{\rm ET} = T_{\rm AR} = T_{\rm CAR} = 1/4$. Therefore, the total electronic transmission coefficient $T_{\rm ET}$ is 5/4, and the AR coefficient $T_{\rm AR}$ and the CAR coefficient $T_{\rm CAR}$ are equal to 1/4.

Figures 4(c) and 4(d) plot the dependence of transmission coefficients on the exchange field λ for different hybridization gaps $m_0 = 0.5$ and -0.5, at the fixed pairing gap $\Delta = 1$. One can see that the Chern number of the topological superconductor is $\mathcal{N} = \pm 2$ for $|\lambda| > 1.5$, $\mathcal{N} = \pm 1$ for $0.5 < |\lambda| < 1.5$, and $\mathcal{N} = 0$ for $|\lambda| < 0.5$. For $|\lambda| < 0.5$, the $\mathcal{N} = 0$ topological superconducting phase exhibits counterpropagating helical Majorana edge states. This helical topological superconductor is analogous to the quantum spin-Hall insulator. As shown in Fig. 3(d), one can find that one-half of the Majorana edge states with opposite chiralities in the quantum spin-Hall terminal region goes through the central scattering region, and the other half of the edge modes are perfectly reflected. Since

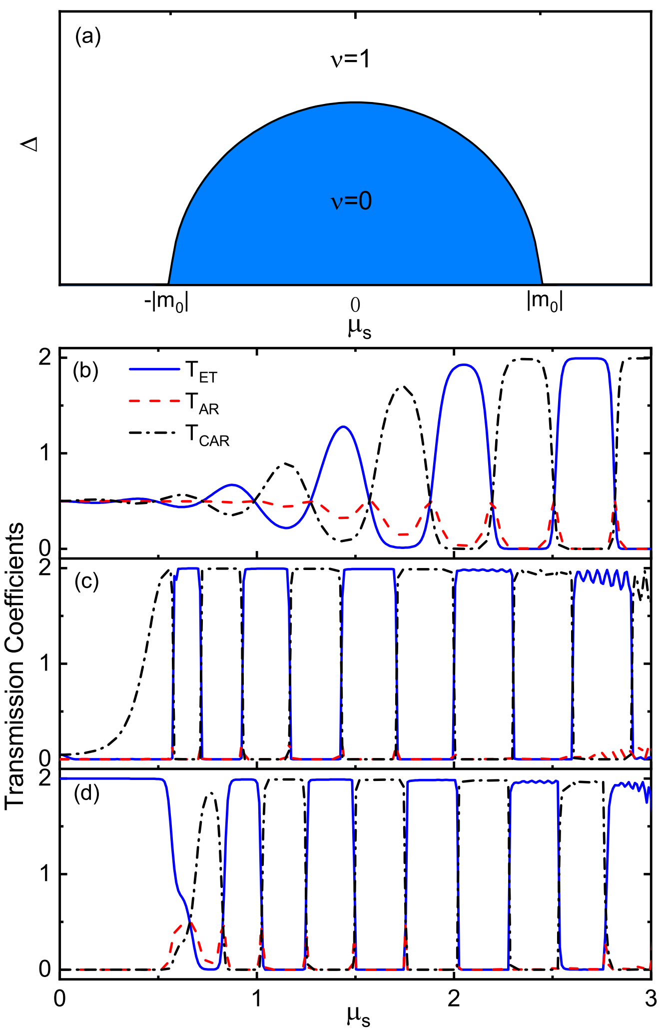

FIG. 5. (a) Phase diagram of the superconducting system for $\lambda = 0$ in the plane of the chemical potential μ_s and the pairing gap Δ. (b–d) Transmission coefficients of electron tunneling $T_{\rm ET}$, Andreev reflection $T_{\rm AR}$, and crossed Andreev reflection $T_{\rm CAR}$ as a function of chemical potential μ_s. $m_0 = 0.5$ and $\Delta = 0.7$ for panel (b), $m_0 = 0.5$ and $\Delta = 0.2$ for panel (c), and $m_0 = -0.5$ and $\Delta = 0.2$ for panel (d). The length of the central TSC is $L = 20$, and the ribbon width is $N = 120$.

the scattering coefficient of the helical topological superconductor is double that of the chiral topological superconductor with Chern number $\mathcal{N} = \pm 1$, we then have $T_{\rm ET} = T_{\rm AR} = T_{\rm CAR} = 1/2$.

In Refs. [52,53], it was shown that a quantized crossed Andreev reflection of $T_{\rm AR} = 1$ can occur in a quantum anomalous Hall insulator proximity coupled with a superconductor. Since the helically propagating edge states of the quantum spin-Hall insulator can be regarded as two copies of the quantum anomalous Hall effect with opposite chiralities, one can easily predict that the crossed Andreev reflection coefficient could be doubled in the system with the quantum spin-Hall insulator proximity coupled with superconductors. To further confirm that the crossed Andreev reflection coefficient is exactly equal to 2, $\lambda = 0$ and $\mu_s \neq 0$ are chosen in Eq. (3). The time-reversal-invariant topological superconductor can be classified by Z_2 invariant ν. As shown in Fig. 5(a), one can see that two quantum phases in the (μ_s, Δ) plane are separated by the boundary of $\Delta^2 + \mu_s^2 = m_0^2$. In the region of $|m_0| > \sqrt{\Delta^2 + \mu_s^2}$, one can get $\nu = 1$, indicating a helical Majorana edge state. In the region of $|m_0| < \sqrt{\Delta^2 + \mu_s^2}$ with $m_0 > 0$, one can get $\nu = 0$, suggesting a trivial superconducting phase. Furthermore, one can obtain a trivial superconducting phase with two pairs of helical edge states in the region of $|m_0| < \sqrt{\Delta^2 + \mu_s^2}$ with $m_0 < 0$. As shown in Figs. 5(b)–5(d), T_{ET}, T_{AR}, and T_{CAR} are dependent on the potential energy μ_s in the quantum spin-Hall insulator–topological superconductor junction. In a narrower topological superconducting region, Majorana fermions can also tunnel between the left and right interfaces of the topological superconductor in addition to the normal propagation along the boundaries of the topological superconductor. To be specific, by increasing μ_s, the phase of the tunneling Majorana fermions can be regulated between zero and π. As a result, the boundary-propagating Majorana fermions and the tunneling Majorana fermions combine together to form electrons or holes, which can emit from the device terminals. Because of the helical nature of the Majorana edge states in our system, the perfect electron tunneling and crossed Andreev reflection can alternately occur with $T_{\mathrm{ET}} = 2$ and $T_{\mathrm{CAR}} = 2$.

V. CONCLUSIONS

We numerically investigated topological phases of the topological superconductor realized by a magnetic topological insulator thin film proximity coupled with two s-wave superconductors on the top and bottom surfaces with opposite pairing gap functions. By adjusting the system parameters, the topological superconductor exhibits rich topological phases which correspond to various Majorana edge modes. In particular, a topological phase with both chiral and helical edge modes can be achieved through a topological phase transition between quantum spin-Hall effect and quantum anomalous Hall effect. We further propose several transport experiments to detect multiple Majorana edge modes. One unique transport signature of the coexisting states with a Chern number of $\mathcal{N} = \pm 1$ is that the coefficient of electron tunneling is quantized to be 5/4 and the remaining scattering probabilities are quantized into 1/4. When the superconductors are proximity coupled with a nonmagnetic topological insulator thin film, by adjusting the chemical potential, the perfectly quantized electron tunneling or crossed Andreev reflection can alternately appear.

ACKNOWLEDGMENTS

This work was financially supported by the National Key Research and Development Program (Grant No. 2017YFB0405703), the National Natural Science Foundation of China (Gants No. 11974327, No. 11474084, No. 11704366 and No. 12074097), Natural Science Foundation of Hebei Province (Grant No. A2020205013), The Fundamental Research Funds for the Central Universities (Grant No. WK2340000087), and Anhui Initiative in Quantum Information Technologies. We also thank the supercomputing service of AM-HPC and the Supercomputing Center of University of Science and Technology of China for providing the high-performance computing resources.

[1] N. Read and D. Green, Phys. Rev. B **61**, 10267 (2000).
[2] X.-L. Qi and S.-C. Zhang, Rev. Mod. Phys. **83**, 1057 (2011).
[3] J. Alicea, Rep. Prog. Phys **75**, 076501 (2012).
[4] C. W. J. Beenakker, Annu. Rev. Condens. Matter Phys. **4**, 113 (2013).
[5] S. R. Elliott and M. Franz, Rev. Mod. Phys. **87**, 137 (2015).
[6] C. Nayak, S. H. Simon, A. Stern, M. Freedman, and S. Das Sarma, Rev. Mod. Phys. **80**, 1083 (2008).
[7] T. Karzig, C. Knapp, R. M. Lutchyn, P. Bonderson, M. B. Hastings, C. Nayak, J. Alicea, K. Flensberg, S. Plugge, Y. Oreg, C. M. Marcus, and M. H. Freedman, Phys. Rev. B **95**, 235305 (2017).
[8] B. Lian, X.-Q. Sun, A. Vaezi, X.-L. Qi, and S.-C. Zhang, Proc. Natl. Acad. Sci. USA **115**, 10938 (2018).
[9] Y.-F. Zhou, Z. Hou, and Q.-F. Sun, Phys. Rev. B **99**, 195137 (2019).
[10] J. D. Sau, R. M. Lutchyn, S. Tewari, and S. Das Sarma, Phys. Rev. Lett **104**, 040502 (2010).
[11] J. Alicea, Phys. Rev. B **81**, 125318 (2010).
[12] S. Nadj-Perge, I. K. Drozdov, B. A. Bernevig, and A. Yazdani, Phys. Rev. B **88**, 020407(R) (2013).
[13] B. Braunecker and P. Simon, Phys. Rev. Lett. **111**, 147202 (2013).
[14] L. Fu and C. L. Kane, Phys. Rev. Lett **100**, 096407 (2008).
[15] A. R. Akhmerov, J. Nilsson, and C. W. J. Beenakker, Phys. Rev. Lett **102**, 216404 (2009).
[16] X.-L. Qi, T.-L. Hughes, and S.-C. Zhang, Phys. Rev. B **82**, 184516 (2010).
[17] S. B. Chung, X.-L. Qi, J. Maciejko, and S.-C. Zhang, Phys. Rev. B **83**, 100512(R) (2011).
[18] J. Wang, Q. Zhou, B. Lian, and S.-C. Zhang, Phys. Rev. B **92**, 064520 (2015).
[19] B. Lian, J. Wang, and S.-C. Zhang, Phys. Rev. B **93**, 161401(R) (2016).
[20] J. Wang and B. Lian, Phys. Rev. Lett **121**, 256801 (2018).
[21] C.-X. Liu, X.-L. Qi, X. Dai, Z. Fang, and S.-C. Zhang, Phys. Rev. Lett **101**, 146802 (2008).
[22] Y. Ren, Z. Qiao, and Q. Niu, Rep. Prog. Phys. **79**, 066501 (2016).
[23] C.-Z. Chang, J. Zhang, X. Feng, J. Shen, Z. Zhang, M. Guo, K. Li, Y. Ou, P. Wei, L.-L. Wang, Z.-Q. Ji, Y. Feng, S. Ji, X. Chen, J. Jia, X. Dai, Z. Fang, S.-C. Zhang, K. He, Y. Wang *et al.*, Science **340**, 167 (2013).
[24] C.-Z. Chang, W. Zhao, D. Y. Kim, H. Zhang, B. A. Assaf, D. Heiman, S.-C. Zhang, C. Liu, M. H. W. Chan, and J. S. Moodera, Nat. Matter. **14**, 473 (2015).
[25] Q. L. He, L. Pan, A. L. Stern, E. C. Burks, X. Che, G. Yin, J. Wang, B. Lin, Q. Zhou, E. S. Choi, K. Murata, X. Kou, Z. Chen, T. Nie, Q. Shao, Y. Fan, S.-C. Zhang, K. Liu, J. Xia, and K. L. Wang, Science **357**, 294 (2017).
[26] W. Ji and X.-G. Wen, Phys. Rev. Lett **120**, 107002 (2018).

[27] Y. Huang, F. Setiawan, and J. D. Sau, Phys. Rev. B **97**, 100501(R) (2018).
[28] M. Kayyalha, D. Xiao, R. Zhang, J. Shin, J. Jiang, F. Wang, Y.-F. Zhao, R. Xiao, L. Zhang, K. M. Fijalkowski, P. Mandal, M. Winnerlein, C. Gould, Q. Li, L. W. Molenkamp, M. H. W. Chan, N. Samarth, and C.-Z. Chang, Science **367**, 64 (2020).
[29] X.-L. Qi, T. L. Hughes, S. Raghu, and S.-C. Zhang, Phys. Rev. Lett **102**, 187001 (2009).
[30] C.-X. Liu and B. Trauzettel, Phys. Rev. B **83**, 220510(R) (2011).
[31] F. Zhang, C. L. Kane, and E. J. Mele, Phys. Rev. Lett **111**, 056402 (2013).
[32] J. Klinovaja, A. Yacoby, and D. Loss, Phys. Rev. B **90**, 155447 (2014).
[33] J. Wang, Phys. Rev. B **94**, 214502 (2016).
[34] Y. Huang and C.-K. Chiu, Phys. Rev. B **98**, 081412(R) (2018).
[35] A. F. Andreev, Zh. Eksp. Teor. Fiz. **46**, 1823 (1964) [Sov. Phys. JETP **19**, 1228 (1964)].
[36] K. T. Law, P. A. Lee, and T. K. Ng, Phys. Rev. Lett. **103**, 237001 (2009).
[37] Q.-F. Sun, Y.-X. Li, W. Long, and J. Wang, Phys. Rev. B **83**, 115315 (2011).
[38] K. Zhang, J. Zeng, Y. Ren, and Z. Qiao, Phys. Rev. B **96**, 085117 (2017).
[39] J. M. Byers and M. E. Flatté, Phys. Rev. Lett **74**, 306 (1995).
[40] J. Nilsson, A. R. Akhmerov, and C. W. J. Beenakker, Phys. Rev. Lett **101**, 120403 (2008).
[41] K. Zhang, J. Zeng, X. Dong, and Q. Chen, J. Phys.: Condens. Matter **30**, 505302 (2018).
[42] M. Veldhorst and A. Brinkman, Phys. Rev. Lett **105**, 107002 (2010).
[43] Y.-T. Zhang, X. Deng, Q.-F. Sun, and Z. Qiao, Sci. Rep. **5**, 14892 (2015).
[44] Z. Hou, Y. Xing, A.-M. Guo, and Q.-F. Sun, Phys. Rev. B **94**, 064516 (2016).
[45] W.-Y. Shan, H.-Z. Lu, and S.-Q. Shen, New J. Phys. **12**, 043048 (2010).
[46] H.-Z. Lu, W.-Y. Shan, W. Yao, Q. Niu, and S.-Q. Shen, Phys. Rev. B **81**, 115407 (2010).
[47] J. Wang, B. Lian, and S.-C. Zhang, Phys. Rev. B **89**, 085106 (2014).
[48] Y. Zeng, C. Lei, G. Chaudhary, and A. H. MacDonald, Phys. Rev. B **97**, 081102(R) (2018).
[49] Q.-F. Sun and X.-C. Xie, J. Phys.: Condens. Matter **21**, 344204 (2009).
[50] J. Wang, B. Lian, and S.-C. Zhang, Phys. Scr. **T164**, 014003 (2015).
[51] Y. Yang, Z. Xu, L. Sheng, B. Wang, D. Y. Xing, and D. N. Sheng, Phys. Rev. Lett. **107**, 066602 (2011).
[52] Y.-T. Zhang, Z. Hou, X. C. Xie, and Q.-F. Sun, Phys. Rev. B **95**, 245433 (2017).
[53] Y.-F. Zhou, Z. Hou, Y.-T. Zhang, and Q.-F. Sun, Phys. Rev. B **97**, 115452 (2018).